Received: 8 October 2022 | Accepted: 12 December 2022

DOI: 10.1002/pamm.202200290

Experiments and Modelling of the Load Capacity of Green Wood

Simon Loske[1,*] and **Ingo Muench**[1]

[1] Institute of Structural Mechanics and Dynamics, Department of Architecture and Civil Engineering, TU Dortmund University

The material properties of green wood in the shaft of vital trees differ significantly from the generally known material properties of technically processed, dried wood. Furthermore, completely different residual stresses and fracture mechanisms are present in the natural full cross-section [1]. The properties also depend on the tree species. Our work focuses on green wood from european beech (Fagus sylvatica). A large number of experiments on small test specimens of green wood are known from [2]. We present both, experiments on small and large-scaled specimens. Latter are bending test on trunks with full cross-section. Combining results and considering micro-mechanical properties of cellular wood components [3], a computational model is fitted to our experimental results. This aspect influences the fracture resistance of a tree and should be representable in a computational model. This is particularly important in order to better assess the risk of building on vital trees.

1 Introduction

The stability of trees is the subject of numerous studies in the forestry and civil sectors, since their failure represents both high material damage and a danger to life and limb. The consideration of this stability becomes particularly interesting when it comes to the structural use of trees. In recent years, more and more structures have been erected around the world, such as observation platforms, tree houses or high ropes courses, where loadings are transmitted to the ground. The structural stability of such a system depends mainly on soil conditions and the utilized trees.Thus, the load capacity of the trees shafts plays a very important role. However, due to the individuality and complexity of trees, the two recognized tree control guidelines ([4, 5]) do not use deterministic models to estimate the load capacity for bending. Although bending mechanism are responsible for the two most common failures: uprooting (foundation failure) of trees and cross-sectional failure in the trees shaft.

2 Failure mechanisms of trees

Two major failure mechanisms are observed in forest stands [6]:

(a) Foundation failure of a tree

(b) Shaft of 6m length in the bending test installation

Fig. 1: Cross-sectional failure of a tree

* Corresponding author: e-mail: simon.loske@tu-dortmund.de, phone +0049 231 755 7302, fax +0049 231 755 6603

Foundation failure The root system of the tree cannot withstand the load as shown in Fig. 1a. This depends mainly on the nature of the soil and the tree species. Uprooting can in principle have three causes: the tensile failure and pulling out of root strands, the lifting of overlying soil layers, and extensive ground failure below the root. Combinations of these effects often occur, whereby factors such as soil moisture content, soil stratification, or damage to the root system from fungal attack or soil compaction are significant. These parameters are difficult to capture and also time variant and highly probabilistic.

Cross-sectional failure This failure depends mainly on material properties of the wood and its geometry. Normal stresses in the shaft become higher, than the materials resistance. The shaft can not withstand the loading (cf. Fig. 1.)

For common conditions we assume, that a tree does not develop mechanical resistance in either the root system or the shaft in very different proportions [7]. Since both failure mechanisms lead to the loss of vitality independently, from arguments of evolutionary theory a tree can only have high fitness if both failure mechanisms are similar. Since cross-sectional failure depends mainly on geometry and material properties of the wood, we consider this case to develop a deterministic model for the prediction of the load capacity.

3 Setup and observations of the bending test

For our bending tests we use whole, freshly cut shafts of european beech (fagus sylvatica) since it is the most widespread deciduous tree in Europe. The stems are destructively tested in a 4-point bending test under laboratory conditions (cf. Fig. 2a). The test-specimen have different shaft diameters varying from $18\,\mathrm{cm}$ to $31\,\mathrm{cm}$.

(a) Shaft of $6\mathrm{m}$ length in the bending test installation

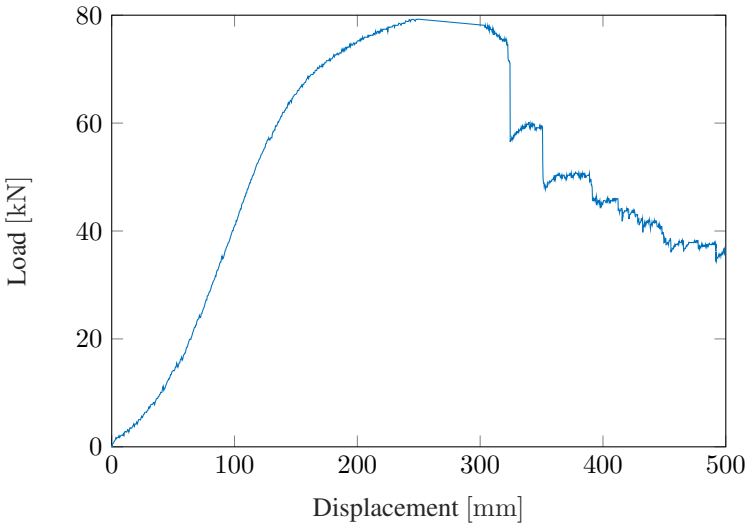

(b) Typical load-displacement curve of bending test

Fig. 2: Bending test installation in laboratory and load-displacement curve

Naturally, the test specimen have to fulfill some criteria. Crucial for the feasibility of bending tests on the shaft is their straightness. Any deviation from straightness implies force eccentricities and additional inhomogeneous stresses in the shaft. We accept 1% deviation from the straight line in relation to the test specimens length. Further we prefer cylindrical shaped shafts, since our deterministic model uses circular cross-section. Since this criterion is not given in the root approach, we take $1.5\mathrm{m}$ long test specimens at least $1.5\mathrm{m}$ above the ground. The first strong branches were above this section, which is another criterion for our selection. We increase the deflection during the test with a servo-hydraulic cylinder in a path-controlled manner at the rate of $50\ \mathrm{mm\,min^{-1}}$ and measure the corresponding force. To ensure the natural moisture conditions in the test-specimens, the shafts are taped at cut surfaces with diffusion-proof foil and tested within three days after felling. Furthermore the shafts are handled carefully to avoid squeezing and cutting of fibers.
The tests show that primary damage appears in the bending pressure zone. Here, local fiber buckling (cf. Fig. 3) resulting in the visible detachment of the bark occurs. This is reflected in a flattening of the load-displacement curve (cf. Fig. 2b), which is linear before. After the load-displacement curve runs horizontally, secondary damage occurs on the bending tension zone. Then, delamination occurs abruptly with simultaneous tearing off individual fiber bundles [8]. It leads to significant

drops in the load-displacement curve. The delaminated fiber bundles form long interlocking tines, shown in Fig. 2b. The final damage mechanism is the delamination of large fiber bundles through the whole cross-section whereby these bundles do not tear.However, for the load capacity of the shaft, this delamination process is not decisive. The local fiber buckling in the bending compression zone and the local tearing off in the bending tension zone determines the maximum in the load-displacement curve. Therefore, we investigate these mechanical properties in further experiments to specify our computation model.

Fig. 3: Local fiber buckling in the bending compression zone

4 Material properties from classical tests

To evaluate the parameters of elasticity, we consider compression and tension tests. Especially the compression test show, that the size of specimens has low impact onto the Young´s modulus and the compressive strength of the material in fiber direction. The same observations holds for the Young´s modulus from tension test, which is the same as for compression in fiber direction. However, the tensile strength of the fibers is so high [9–11] that we were only able to determine it inadequately even with large clamping areas of the test specimens. Therefore, the tensile strength in the fiber direction is introduced as a parameter in the following calculation model, which is derived from the data points of the bending tests.

5 Setup of the computational model and results

The calculation model is set up based on a stress distribution in the cross-section subjected to bending. The 3-dimensional stress state in the cross-section of the shaft is reduced to the component σ_x in the longitudinal direction for the simplified calculation model, shown in Fig. 4. For pure bending around the ξ-axis, we neglect its variability in the ξ-direction. We assume the normal stress field σ_x of each circular cross-section V as nonlinear function of polynomial order $\mathbb{P}^3(\eta)$ in the compression zone and $\mathbb{P}^1(\eta)$ in the tension zone for bending around the ξ-axis. The edge of the shaft represents the integration limits

$$\xi_\Gamma^2 + \eta_\Gamma^2 = R^2 \tag{1}$$

of the stress function σ_x. For pure bending, this is subject to the constraint

$$\int_{\xi=0}^{\xi_\Gamma} \int_{\eta=0}^{\eta_\Gamma} \sigma_x(\eta)\, \mathrm{d}\xi \mathrm{d}\eta = 0 \quad \text{with} \quad \sigma_x = \begin{cases} c_1\eta^3 + c_2\eta^2 + c_3\eta + c_4, & -R \le \eta \le \eta_0 \\ c_5\eta + c_6, & \eta_0 \le \eta \le +R \end{cases} \tag{2}$$

from the balance of linear momentum in the longitudinal direction. The bending moment reads

$$M = \int_{\xi=0}^{\xi_\Gamma} \int_{\eta=0}^{\eta_\Gamma} \sigma_x(\eta)\eta \, \mathrm{d}\xi \mathrm{d}\eta, \tag{3}$$

with the boundary/transition conditions

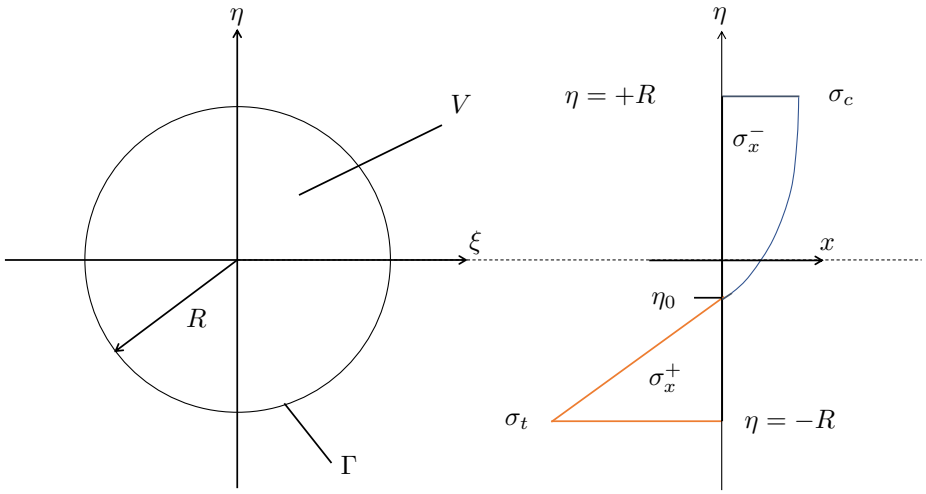

Fig. 4: Computational model of cross-section stress distribution

$$\begin{array}{lll} \sigma_x(\eta=-R)=\sigma_t, & \sigma_x(\eta=\eta_0)=0, & \sigma_x(\eta=+R)=\sigma_c, \\ \sigma_x'(\eta=+R)=0, & \sigma_x(\eta=\eta_0^+)=\sigma_x(\eta=\eta_0^-), & \sigma_x'(\eta=\eta_0^+)=\sigma_x'(\eta=\eta_0^-). \end{array} \tag{4}$$

We use Eq. 2 and Eq. 4 to the stress function depending on the parameters σ_t, σ_c and η_0

$$\sigma_x(\eta,\eta_0,\sigma_t)=\begin{cases} \left(\frac{-\sigma_t}{(2R-\eta_0)\eta_0^2}+\frac{2\sigma_c}{\eta_0^3}\right)\eta^3-\left(\frac{-\sigma_t}{(2R-\eta_0)\eta_0}+\frac{3\sigma_c}{\eta_0^2}\right)\eta^2+\sigma_c, & -R\le\eta\le\eta_0 \\ \frac{-\sigma_t}{2R-\eta_0}\eta+\frac{\sigma_t\eta_0}{2R-\eta_0}, & \eta_0\le\eta\le+R, \end{cases} \tag{5}$$

where the compressive stress σ_c is given by experiments, the position of the stress zero line η_0 has to be determined iterative under equilibrium condition from Eq. (2) and σ_t is the missing target value which is to be adapted to the results of the bending tests by curve fitting. The convergence of curve fitting is shown in Fig. 5a.

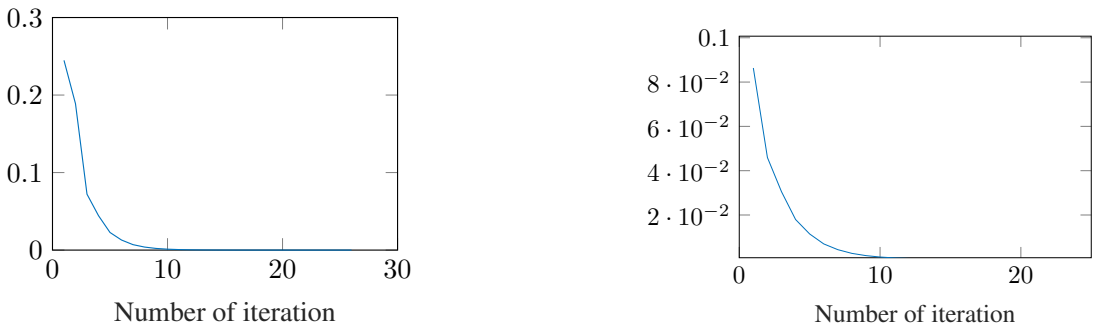

(a) Relative error in calculation of σ_t

(b) Relative error in calculation of η_0 for given σ_t

Fig. 5: Convergence behavior of iterative model calculation

The fitted curve is calculated by interval bisecting method af a conceivable interval for the tension stiffness σ_t with $\sigma_c \le \sigma_t \le 3\sigma_c$. The objective function is the minimization of variance between computational model bending moment calculated by Eq. (3) an experimental bending moment measured in the L_1 norm. Results of 16 bending experiments can be considered in

$$\min_{\sigma_t\in[\sigma_c,3\sigma_c]} \sum_{k=1}^{16} \left\| M_{exp}(R(k)) - M_{comp}(R(k),\sigma_t,\eta_0) \right\|_1 \tag{6}$$

with the bending moment load capacity from the experimental data M_{exp} for different discrete shaft radius R and the corresponding calculated moment M_{comp}. In each iteration step the equilibrium condition from Eq. (2) is solved with a predictor-corrector method to obtain η_0. Therefor an initial value of $\eta_{0,1} = 0$ is chosen. The corrector is formulated with a linear approximation to Eq. (2) in the correction range. Thereby the balance of linear momentum gives the direction of the corrector step

$$\eta_{0,i+1} = \eta_{0,i} + \frac{\int_{\xi=0}^{\xi_\Gamma} \int_{\eta=0}^{\eta_\Gamma} \sigma_x(\eta) \, \mathrm{d}\xi \mathrm{d}\eta}{\int_{\xi=0}^{\xi_\Gamma} \int_{\eta=0}^{\eta_\Gamma} \|\sigma_x(\eta)\|_2 \, \mathrm{d}\xi \mathrm{d}\eta} \left(2R - \eta_{0,i}\right). \tag{7}$$

The convergence is exemplified for a single calculation of the associated η_0 for a given σ_t shown in Fig. 5b. Integrations are implemented numerically via a trapezoidal method.
With the bending moment load capacity for different shafts from our experiments and our measured compression strength of $\sigma_c = 33\mathrm{MPa}$ the curve fitting provides a corresponding tension strength of $\sigma_t = 83\mathrm{MPa}$. Finally the fitted curve is given in comparison to the experimental results in Fig. 6. Also the comparison to an assumption of linear elastic behavior with $\sigma_t = \sigma_c$ (state before first damage in pressure zone) is shown.

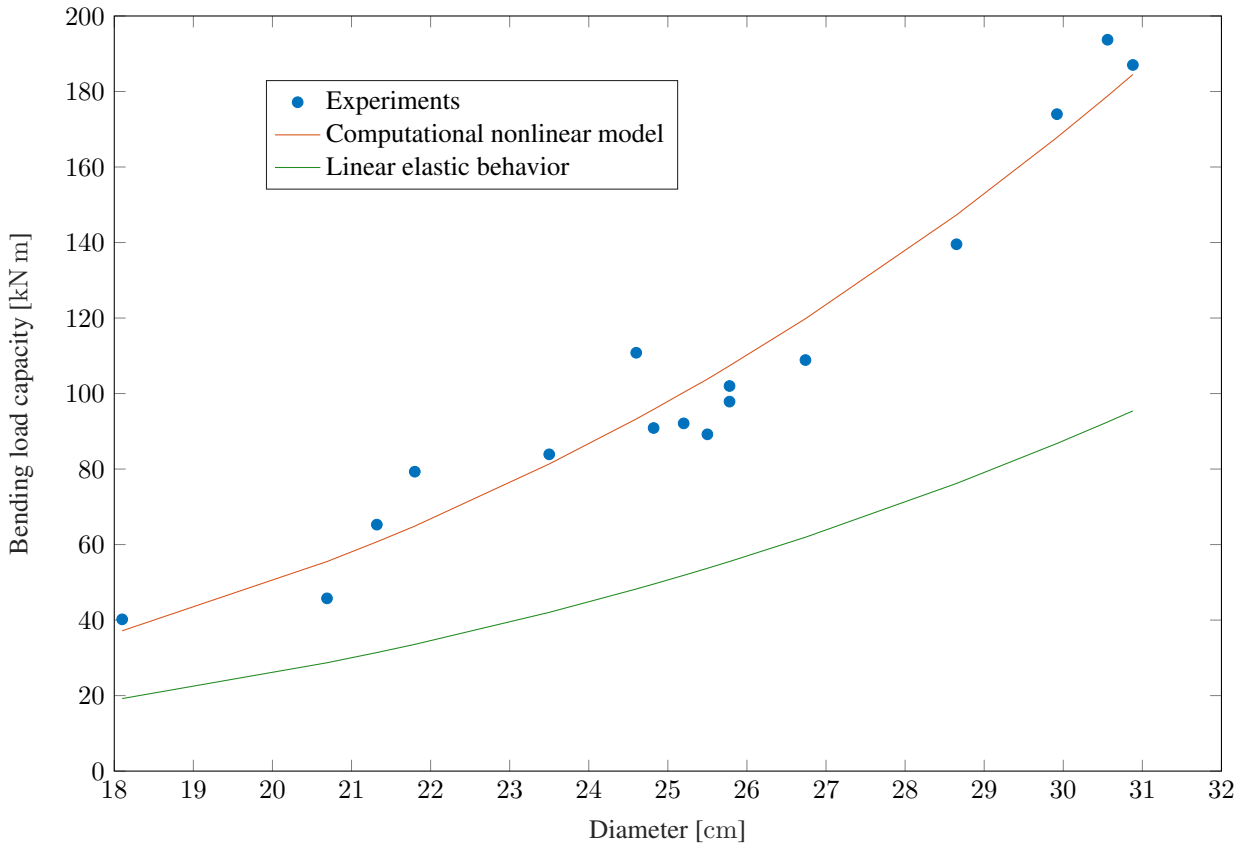

Fig. 6: Bending moment load capacity

6 Conclusions

With the established calculation model, it is possible to determine the tensile strength of the wood based on the results of bending tests and compression tests. With these complete material parameters, the load-bearing capacity of trees can be extrapolated and predicted from the determined test data. Attempts should be made to verify the material parameters thus determined by further experimental investigations and thus to substantiate the stress hypothesis established.

Acknowledgements Open access funding enabled and organized by Projekt DEAL.

References

[1] K. Niklas and H. C. Spatz, American Journal of Botany **97**(10), 1587–1594 (2010).
[2] G. Lavers, The strength properties of timber. her majesty's stationary office, 1969.
[3] X. Zhang, J. Li, Z. Yu, Y. Yu, and H. Wang, Journal of Materials Science **52**(12), 6999–7007 (2017).
[4] Baumkontrollrichtlinien für regelkontrollen zur Überprüfung der verkehrssicherheit von bäumen – baumkontrollrichtlinien, Tech. rep., Forschungsgesellschaft Landschaftsentwicklung Landschaftsbau e.V., 2010.
[5] M. Erb and L. Wessolly, Manual of tree statics and tree inspection, 2016.
[6] B. Gardiner, K. Byrne, S. Hale, K. Kamimura, S. Mitchell, H. Peltola, and J. C. Ruel, Forestry **81**(3), 447–463 (2008).
[7] C. Mattheck, K. Bethge, and D. Erb, Arboricultural Journal **17**(2), 201–209 (1993).
[8] L. Donaldson, in: Delamination of Wood at the Microscopic Scale: Current Knowledge and Methods (Springer Netherlands, 2010), pp. 123–144.
[9] Wood handbook-wood as an engineering material, Tech. rep., Madison, WI, 2010.
[10] U. Büyüksarı, N. As, T. Dundar, and O. Korkmaz, Ciencia y Tecnología **19**, 481–494 (2017).
[11] The relationship between the anatomy and mechanical properties of different green wood species a thesis submitted to the university of manchester for the degree of doctor of philosophy in the faculty of life sciences, 2015.